Photoluminescence quenching processes by NO2 adsorption in ZnO nanostructured films

ARTICLE *in* JOURNAL OF APPLIED PHYSICS · APRIL 2012

Impact Factor: 2.18 · DOI: 10.1063/1.3700251

Photoluminescence quenching processes by NO_2 adsorption in ZnO nanostructured films

A. Cretì,[1,a)] D. Valerini,[2] A. Taurino,[1] F. Quaranta,[1] M. Lomascolo,[1] and R. Rella[1]
[1]*IMM – CNR, Institute for Microelectronics and Microsystems, Campus Universitario, Via per Monteroni, 73100 Lecce, Italy*
[2]*ENEA, UTTMATB, Brindisi Research Center, S.S. 7 Appia - km 706, 72100 Brindisi, Italy*

(Received 6 October 2011; accepted 5 March 2012; published online 9 April 2012)

The optical response by NO_2 gas adsorption at different concentrations has been investigated, at room temperature, in ZnO nanostructured films grown by controlled vapor phase deposition. The variation (quenching) in the photoluminescence signal from excitonic and defects bands, due to the interactions between the oxidizing gas molecules and the sample surface, has been detected and dynamic responses and calibration curves as a function of gas concentration have been obtained and analyzed for each band. We showed that the sensing response results larger in excitonic band than in defect one and that the emission signal rises from two different quenchable and unquenchable states. A simple model was proposed in order to explain the quenching processes on the emission intensity and to correlate them to the morphological features of the samples. Finally, the reversibility of the quenching effects has also been tested at high gas concentration. © *2012 American Institute of Physics.* [http://dx.doi.org/10.1063/1.3700251]

I. INTRODUCTION

Today nanostructured semiconductor oxide materials arouse great interest due to their potentially wide range of application in electronics, opto-electronics and photonics.[1–3]

In particular, the synthesis of ZnO thin films, nanocrystals and nanowires with size up to a few hundreds of nanometers have induced a rapid advancement in many areas such as gas sensors, biosensors, transducers, catalysis, lasers, etc.[4–10] This is due to the fact that these materials exhibit chemical and physical properties that differ from the corresponding bulk ones, due to both quantum size effects (if the dimensions are below 7 nm)[11–13] and to the high surface/volume ratio. Optical and electron-transport properties of ZnO nanostructured materials are interesting for sensing applications. The presence of oxygen vacancies and other typical defects is responsible of their catalytical properties and makes these materials sensible to the adsorption of different analytes. Several studies have shown that ZnO nanostructured thick films, nanoparticles and nanowires exhibit sensing response to Volatile Organic Compounds CO, NO_2, H_2, NH_3, O_3 gases and can be used as pH sensors,[14–18] mainly monitored by electrical measurements. As gas sensing material, based on the near-surface modification of electron density distribution in presence of suitable surface-absorbed species, ZnO nanostructured films provide significant enhancements in sensitivity due to their high surface-to-volume ratio. Recently the properties of ZnO nanostructures have been also explored in the optical chemical sensor field.[19–23] Mazingue *et al*., for example, used the m-lines technique[22] to detect butane gas by using nanostructured ZnO films. Gas sensing tests based on the ZnO optical properties have been performed by the Surface Plasmon Resonance technique,[21] by using optical fibers,[23] or by measurements of photoluminescence (PL) emission variations in presence/absence of analyte gas molecules. The PL-based sensors result attractive because they can provide stability, good sensitivity, and a rapid, reproducible, and reversible response, at room temperature.

Concerning the chemical sensing in presence of NO_2 gas molecules, different experimental and theoretical studies have been performed in order to clarified the surface interaction.[24,25] In fact, several adsorption processes can occur and consequently the electron trapping can manifest oneself in different ways. The sensing response has been strongly investigated by electrical measurements. Recently the optical chemical sensing has been explored and measurements of PL variations in presence/absence of analyte gas molecules have been performed.[19,20] However the PL quenching processes induced by the gas molecules interactions and the role of morphological and structural properties of the sample on the adsorption processes have not been extensively investigated.

In this paper, the variations of the PL emission of thick nanostructured films of ZnO nanowires has been investigated at room temperature in presence/absence of NO_2 gas molecules, in the excitonic and defect emission band,[26] in order to study the mechanisms involved in the PL quenching and to evaluate the material suitability in optical sensing applications. In particular the role of the sample features in the quenching processes is analyzed. The investigated film has been grown by a vapor phase deposition (VPD) route on sapphire substrate. Scanning electron microscopy (SEM), X-ray diffraction (XRD), and PL measurements at low (7 K), and room temperature (RT) have been performed to assess the sample quality. Details about the sample preparation and the morphological, structural, and optical characterization have been reported.

The PL signal of the films has been monitored in presence of NO_2 molecules, one of the major toxic air pollutants, mixed in nitrogen, at different gas concentrations from 25 to

a)Author to whom correspondence should be addressed. Electronic mail: arianna.creti@le.imm.cnr.it.

115 ppm, in the excitonic and defect emission band.[26] In this paper we focused on the interaction between ZnO material and the NO_2 oxidizing species, due to the intrinsic n-type doping behavior of the semiconductor material. In fact, lattice defects like oxygen vacancies and zinc interstitials, in the ZnO material, can act as electron donors in presence of oxidizing gas, decreasing the number of charge-carriers that can radiatively recombine.

In order to explain the observed photoluminescence quenching behavior in the samples, a simple model has been proposed. In particular, we demonstrated that the interactions between gas molecules and sample surface, which induce the PL signal reduction, involve mainly the surface of the nanowires, which stacked from the buffer layer. The buffer layer emission signal, in fact, results unaffected by quenching mechanisms because the nanowires, forming a surface network, strongly reduce the diffusivity paths for gas molecules, preventing their interactions with the surface of the buffer layer.

II. EXPERIMENTAL DETAILS

The ZnO nanostructured films investigated in this paper have been grown on sapphire substrate by VPD growth technique, in a conventional furnace with horizontal quartz tube (25 mm inner diameter). Zn 5 N pure granular Zn source was placed in a tungsten crucible and inserted in the furnace at room temperature. The substrate was placed in front of the crucible at a distance of 10 mm, and 5 N Ar was used as carrier gas with a flux of 1 ml/min. The temperature ramp started after five minutes of gas flux. The furnace was heated up to 600 °C in 10 min, maintained at this temperature during the deposition for 60 min and then slowly cooled down to room temperature. Site-selective nucleation and growth of ZnO nanocrystals was achieved by coating the substrate with Au islands by e-beam evaporation. For a nominal Au film thickness of 3 nm discontinuous Au islands were obtained. On these small metal islands, a nanowire growth was observed.

A JEOL 6500 F Scanning Electron Microscope was used to analyze the surface morphology of the samples and X-ray diffraction measurements were performed in the θ-2θ geometry by using the CuKα excitation line ($\lambda = 1.5402$ Å) of a Rigaku diffractometer.

Photoluminescence measurements at low (7 K) and room temperature, were carried out by He-Cd laser (325 nm), at low pump intensity ($\sim$50 W/cm^2), and dispersed by a 0.3 m focal length monocromator Jobin-Yvon Mod TRIAX 320, equipped with a 1200 lines/mm grating blazed at 330 nm, with a nominal spectral dispersion of 2.64 nm/mm @500 nm. This gives an energy resolution in the recording PL spectra of about 0.5 meV in UV range. Finally the PL has been detected by cooled GaAs photomultiplier operating in photon-counting mode.

Finally, for the PL quenching measurements, the samples were placed inside an atmosphere-controlled sealed chamber and exposed to the gas analyte mixed in nitrogen. The chamber was provided with four apertures: Two apertures were used for gas inlet and outlet, respectively, and the others were connected with two optical fibers for the PL excitation and collection. The collected PL emission was sent to a spectrometer (Avantes MC2000) with a 75 mm focal length and a CCD linear array detector. The software (Avantes SpectraWin5) allowed us to acquire the integral of the PL spectrum in a fixed wavelength range at a fixed time interval.

The variation of the excitation intensity during the run-time measurements was monitored by using a Si detector in order to normalize the response curves. The gas mixing station consisted of a mass flow controller (Brooks Instruments 5850S) equipped with three mass flow meters/controllers operating in the range 2.5-50 ml/min and a system of Teflon pipelines and switching valves. The measurements were performed at room temperature.

In order to monitor the dynamical optical sensing properties of the nanostructured ZnO films, the sensing tests were performed sending in the test chamber a controlled flow of nitrogen as carrier gas in order to acquire the signal baseline and, successively, a controlled mixture of the investigated gas molecules (NO_2) in nitrogen, maintaining the total flow in the test chamber at 50 ml/min. The bottle of NO_2 gas at certified concentration contains dry-air as carrier gas.

In our experiment we have considered the possibility that the reduced PL intensity was due to the direct interaction between the NO_2 molecules and the UV photons, inducing photo dissociation in the gas,[27,28] but a suitable experimental control allows us to exclude this case (see in Ref. 29).

III. RESULTS AND DISCUSSION

A. Morphological, structural, and optical properties

As shown by the SEM image in Fig. 1, the investigated samples consist of nanowires with a large diameter and quite

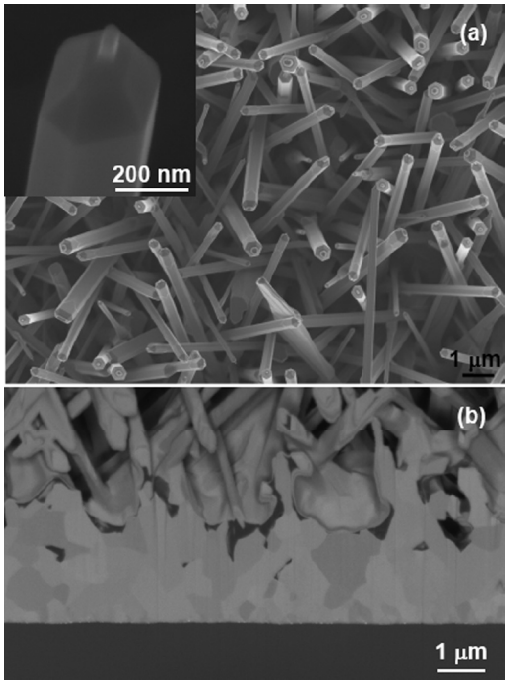

FIG. 1. SEM images corresponding to a typical morphology of ZnO nanostructured film. (a) Top view image of the film and (inset) magnified image of a single nanorod showing the tip tapering; (b) cross sectional image of sample showing the buffer layer under the nanorods.

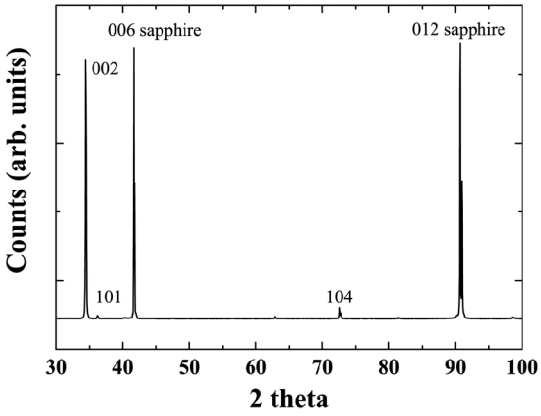

FIG. 2. Typical X-ray diffraction spectrum obtained from ZnO nanostructured films grown on a sapphire substrate.

wide size dispersion, ranging between 250 and 500 nm. High resolution SEM analysis revealed that the nanowires have a hexagonal section and a tapered tip, with a strongly sharpened end, as shown in the inset of Fig. 1(a); SEM cross sectional investigations demonstrated that the nanowires stuck on a buffer layer of randomly oriented ZnO polycrystals, few micrometers thick, as visible in Fig. 1(b) (see also in Ref. 30).

The crystal quality of the films has been investigated by X-ray diffraction (XRD). The typical θ-2θ XRD spectrum of the samples (reported in Fig. 2) indicates that the crystal structure is hexagonal (wurtzite, JCPDS 36-1451); the spectrum shows a very intense ZnO 002 peak indicating a good structural quality. Evidence of much weaker secondary peaks (101 and 104) is also present.

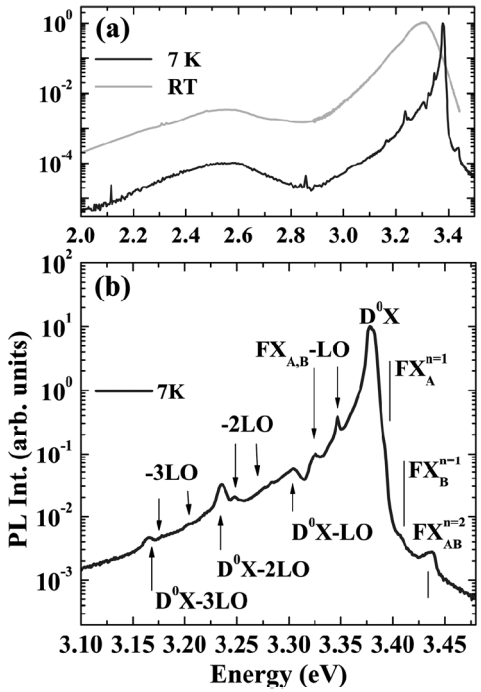

FIG. 3. Comparison between the tipycal PL spectra at 7K and at room temperature of the samples (a) and zoom of excitonic emission band spectrum detected at low temperature (b). The label "LO" denotes the phonon replicas due to the longitudinal optical phonons.

Figure 3(a) shows the typical PL spectrum of the samples at low (7 K) and at room temperature. The low-temperature PL measurements allow us to assess the crystal quality of the samples. In particular, the excitonic emission signal (Fig. 3(b)), as discussed later, presents the typical characteristics related to a good crystal quality, as widely discussed in the literature[26,31–36] that are (1) the observation of a free exciton emission narrow-band; (2) the spectrally resolved fine structure of exciton states (A and B excitons); (3) the observation of spectroscopic signature associated with high order ($n \geq 2$) free exciton PL features.

The PL signal ranges from the visible range (green-orange) to the UV-region. In particular, the visible signal, due to defect emission and usually attributed to oxygen vacancies (green emission) and/or interstitial oxygen (orange emission),[37] results one (at RT) or more (at low temperature) orders of magnitude smaller than the UV signal, due to the band-edge emission, thus suggesting a low defect density presence and then a good structural quality.

Rigorously it is not obvious to evaluate the structural quality of the sample from the intensity ratio between the visible signal and the UV one, because this value is dependent on sample type and on excitation density, as shown for example by Shi *et al.*[38] Nevertheless in our case the high quality is confirmed by the structured excitonic emission spectra detected at low temperature reported in Fig. 3(b). In more details, we can see that a typical exciton bound to a donor level (D^0X) at $\sim$3.38 eV and the free exciton (FX_A) transition, at 3.392 eV, dominate the spectrum;[39] the D^0X phonon replicas are also well evident. In particular, the D^0X transition is split in two different structures (3.377 eV and 3.381 eV), separated of about 4 meV,[39] and there is strong evidence of the phonon replicas of both D^0X and FX transitions. In the high energy region of this spectrum the FX_B state[26] and the first excited states of FX_A and FX_B (FX_{AB}) transitions[26] result also visible. Furthermore in the phonon replica of the free exciton transition, it is possible to distinguish the replica of FX_A from the one of FX_B transition. (The emission signal at 3.35 eV can be also attributed to the typical two-electron satellite (TES) recombination.[39])

As visible in Fig. 3(a), at room temperature the UV emission band results broadened, as expected to the increased phonon scattering events, and red-shifted with respect to the corresponding one observed at 7 K, as expected, in agreement with the Varshni law.[40]

At low energy the PL spectrum, related to defects emission, is characterized by a broad band whose spectral range is not affected by the sample temperature. This band is centered at 2.5 eV and extends from the blue to the green range, with a small tail in the orange region. To take into account these defect band features and to have more information about their origin, in order to correlate them to the sensing response (see later in the text), we fitted the PL curve in this range, at each temperature, with a sum of more Gaussian bands. The best fit involved 3 bands centered at 2.33, 2.55, and 2.84 eV, respectively. The predominant signal in the defect band was represented by the band at 2.55 eV, usually ascribed to oxygen vacancies V_O.[41,42] The other two bands present in the blue region (2.84 eV) and at lower energy

(2.33 eV) indicate the presence of interstitial zinc I_{Zn} (Ref. 43) and interstitial oxygen I_O (Ref. 42), respectively. These attributions allowed us to distinguish the contribution of donor-related (DL) and of acceptor-related (AL) defects emission to the PL signal.[44] In conclusion, we can state that the larger contribution to the defect emission signal is due to V_O and I_{Zn} defect states, therefore to DL emission and we can correlate these information to the sensing response of the samples.

B. Sensing test

The variation of the PL emission due to NO_2 gas interaction (adsorption) on the surface of the ZnO nanostructures, has been investigated. Usually the presence of NO_2 gas molecules induces a PL quenching in ZnO nanostructures, due to the decrease in the number of charge-carriers that can recombine radiatively. In fact, ZnO material is an intrinsic n-type semiconductor, due to native lattice defects like oxygen vacancies and zinc interstitials, which act as electron donors in presence of oxidizing species like NO_2. Nevertheless, the interaction between NO_2 molecules and ZnO surface is not a simple subject, because several adsorption processes can occur and the electron trapping can happen in different ways and by different reactions (for more details, see Ref. 29).

The trapping of electrons at the gas adsorption sites and the generation of a depletion layer for charge-carriers on the ZnO material surface, induce a PL signal reduction. The recovery is possible if the adsorption processes are reversible and the adsorbed molecules, in presence of an inert atmosphere, leave the surface, allowing the de-trapping of electrons.

In Fig. 4 the typical normalized dynamic response signals due to the quenching/recovery of the integrated luminescence signal of the samples are shown for the two investigated spectral regions, corresponding to excitonic (from 3.10 to 3.44 eV) and defects (from 2.07 to 2.75 eV) emission bands.

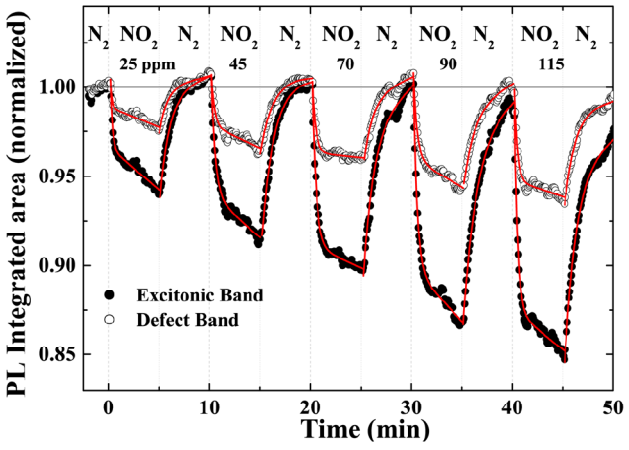

FIG. 4. Optical sensing measurements at different NO_2 gas concentration (total flow of 50 ml/min) and at nitrogen recovery atmosphere, for excitonic (filled circle) and defect emission (empty circle) band of sample. The best fits (continuous lines) obtained by the fitting function of each quenching/recovery cycle $I = A\exp\left[\frac{-(t-t_0)}{\tau}\right] + Bt + y_0$, where I stands for the integrated photoluminescence intensity, t represents the time, t_0 is the time corresponding to the edge of quenching/recovery cycle, τ is the time constant of the exponential process, y_0 is an offset fit parameter, are also shown.

The dynamic response signals have been detected at different gas concentration, ranging from 25 ppm to 115 ppm. Before the measurements, the nanowires have been exposed only to flow of nitrogen atmosphere, in order to acquire the baseline of the measure, as previously explained.

In order to give a quantitative evaluation of the quenching process, the calibration curves are derived from the dynamic response signals. The calibration curves represent the variation of the PL intensity signal when the sample is exposed to a gas atmosphere (N_2 or dry-air, for example) or to a given gas concentration mixed in the carrier gas (NO_2 in N_2 in our case), normalized to the baseline value. After all, in the calibration curves (as we will see later in the text and in the Fig. 5(a)), the sensor response R, defined as the percentage variation of the PL intensity, is plotted as a function of gas concentration:

$$R([Q]) = \frac{\Delta I}{I}\% = \frac{I_0 - I_{gas}}{I_0}, \tag{1}$$

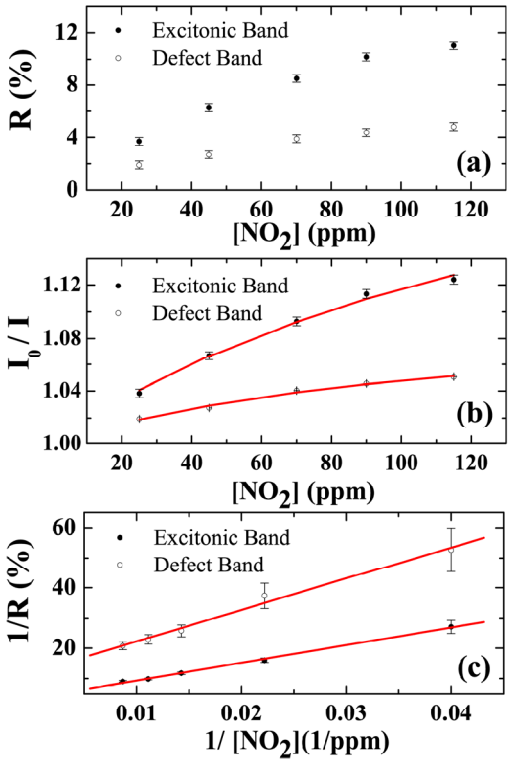

FIG. 5. (a) Calibration curves of excitonic (filled circle) and defect emission (empty circle) band response signal. (b) Stern-Volmer plots and best fit (continuous lines) of excitonic (filled circle) and defect band (empty circle) emission signal by the modified Stern-Volmer equation $\frac{I_0}{I} = \left[\sum_{i=1}^{n} \frac{f_{(i)}}{(1+K_{SV(i)}[Q])}\right]^{-1}$, where it is assumed that n fluorescent multiple species, independent and not interacting one another, are present in the sensing material. In the equation (i) denotes a specific K_{SV} value per species, and $f_{(i)}$ is the fractional intensity of each emitting species. (c) 1/R dependence on 1/[NO_2] and best fit (continuous lines) of excitonic (filled circle) and defect band (empty circle) emission signal by using equation $\frac{I_0}{\Delta I} = \frac{1}{R[Q]} = \frac{1}{f_a K_{SV}^q [Q]} + \frac{1}{f_a}$, where I_0^q and I_0^{un} are the PL intensities of the quenched and unquenched emitters, respectively, and f_a is the quenchable fraction of the initial PL signal, namely, $f_a = \frac{I_0^q}{I_0^q + I_0^{un}}$.

where [Q] is the gas molecules concentration and, in each quenching cycle, I_0 stands for the integrated PL intensity at t_0 (start time), namely the baseline value, and I_{gas} stands for the equilibrium value of integrated PL signal achieved in each response cycle.

In our case, we can derive the calibration curves from the dynamic response signals of both excitonic and defect emission bands in order to compare their sensitivity. However we observe that 5 min are enough to allow the recovery of the signal in nitrogen atmosphere and then to define the I_0 value in each cycle, but this time range is not enough to reach an equilibrium value of the response signal and then to define I_{gas} value. In fact in each cycle the response signal shows a fast reduction in the first minute followed by a slow signal decrease as the exposure time increases. A longer gas exposure up to 20 min (not shown) at the higher gas concentration (115 ppm) shows the same trend. Then we can deduce that the interactions between the sample surface and the gas molecules take place by means of different processes characterized by different kinetics. In particular a very slow kinetic seems to justify the absence of reached equilibrium value in the investigated time ranges.

In order to define and estimate the response signal in each cycle and to clarify the interaction processes between gas molecules and film we have analyzed the response/recovery curves by means of an appropriate fitting procedure. It results that the number of involved suitable adsorption sites during the exposure to the gas molecules (restoring atmosphere) decreases (increases) exponentially as the time increases by means of two different time constants. In particular, since the longer time constant exceeds the investigated response/recovery time range, we replaced the corresponding exponential function, in the fitting function, with its first-order series expansion (that is a linear function). As a consequence we defined the fitting function of each quenching/recovery cycle as

$$I = A \exp\left[\frac{-(t - t_0)}{\tau}\right] + Bt + y_0, \qquad (2)$$

where I stands for the integrated photoluminescence intensity, t represents the time, t_0 is the time corresponding to the edge of quenching/recovery cycle, τ is the time constant of the exponential process, y_0 is an offset fit parameter that varies in the range from 0.8 to 1.0, and A and B are fitting parameters. The best fits are represented by the continuous lines in Fig. 4.

The exponential contribution acts as decay ($A > 0$) or as recovery ($A < 0$), and it results from the interaction processes between the quenchable surface sites and the gas molecules, which induces the rapid decreases (increases) of the integrated PL signal in presence (absence) of the gas. The linear part of the fitting function, on the contrary, allows one to estimate, in each cycle, the contribution of the slower processes to the sensing response ($B < 0$)/recovery ($B > 0$) signal.

The values of A and B reported in Table I are the weighted average value and the related standard deviation, obtained from the fitting procedure in the different cycles (that is at different gas concentrations) for the excitonic and defect band signals. We observe that the B values result to be about two order of magnitude smaller than the A values one (B/A ~3%) suggesting that the response/recovery signal in the sensing test is determined mainly from the fast interactions. As a consequence we consider the decay (recovery) time constant τ an estimation of the rapidity of the sample response (recovery), which allows us to evaluate the response (recovery) time of the sensing test, defined in general as the time necessary to induce a reduction (recovery) of 90% of the signal.

The weighted average value and the related standard deviation of the decay and recovery time constants, resulting from the fitting procedure of the signal detected at the different gas molecules concentration, are reported in Table I, together with the following response and recovery times, for both excitonic and defect band signals. We observe that they are almost the same in the excitonic and defect emission band dynamics, suggesting that the fast interaction mechanism is the same in both bands.

In this frame, in order to derive the calibration curves, we can assume as response signal I_{gas} the signal value corresponding at the calculated response time, then neglecting the contribution of the slow process. In this regard we stress that the decrease of the signal induced by the slower process results of about 1.4-3.5% (0.3-1.8%) of the I_{gas} value in

TABLE I. Average value of the decay (recovery) time constants, response (recovery) times and fitting parameters A and B of response (recovery) cycles of excitonic and defect emission band resulting by the fitting procedure.

	Average value			
	Response cycles		Recovery cycles	
	A>0	B>0	A<0	B<0
Excitonic Band	0.150 ± 0.002	0.0042 ± 0.0001	0.095 ± 0.001	0.00405 ± 0.00001
Defect band	0.076 ± 0.002	0.0019 ± 0.0001	0.042 ± 0.001	0.0017 ± 0.0003
	Average value (min)			
	Decay time constant (τ)	Response time	Recovery time constant (τ)	Recovery time
Excitonic band	0.33 ± 0.01	0.80 ± 0.02	1.13 ± 0.02	2.75 ± 0.05
Defect band	0.29 ± 0.01	0.71 ± 0.03	1.11 ± 0.03	2.70 ± 0.09

excitonic (defect) band signal dynamic (percentage estimated by $\frac{B\Delta t}{I_{gas}}$ where Δt is the gas exposure time period) and it does not depend on gas molecules concentration. The same assumption can be made for the recovery cycles, which exhibit even smaller percentage variations respect to the I_0 value (1.0-3.0% and 0.7-1.4% in excitonic and defect band cycles, respectively).

The resulting calibration curves are reported in Fig. 5(a). We observe that the sensing response R in excitonic (R_{exc}) and defect emission (R_{def}) bands increases as the gas molecules concentration increases, meaning that the quenching effect increases with the gas concentration. This quenching increment shows a sub linear trend in the investigated range. The different R values observed in the excitonic and defect band can be ascribed to the different nature of emission and recombination processes in the two bands, as previously discussed. The excitonic band is due to recombination by free and bound exciton states, which result more delocalized in the sample than the defect ones. As R_{exc} is higher than R_{def}, then we can conclude that the exciton states result more affected by surface interaction than the defect ones. However in order to better understand the quenching mechanisms in the PL signal, further and accurate investigations should be performed, in both emission bands, when interaction between gas molecules and surface sensing layer occurs.

We observe that in general the quenching process in isotropic 3-D medium usually obeys the Stern-Volmer equation[45]:

$$\frac{I_0}{I} = 1 + K_{SV}[Q], \tag{3}$$

where I_0 and I stand for the PL intensity in the absence and in the presence of the quencher, respectively, [Q] is the quencher concentration, and the Stern-Volmer constant K_{SV} assumes a different meaning in the case of static or dynamic quenching. In particular the PL quenching process is static when the interaction occurs before the photo-excitation of the emission state, and it is dynamic when the photochemical process results by collision between the photo-excited material and the quencher species. In the first case, the quenching process induces a decrease in the number of available radiative states without modifications of the decay rates, whereas in the second case it affects the PL lifetimes.[45,46] Then in the case of dynamic quenching K_{SV} is the product of the unquenched excited state lifetime and the bimolecular quenching rate constant. When the static quenching is the only luminescent deactivation mechanism, Eq. (3) still provides a description of the interaction and in this case K_{SV} is the association constant K_{as} of the static process.

Anyway, different factors can induce strong departure from the linearity given by the Stern-Volmer equation. Usually both static and dynamic mechanisms can operate simultaneously and then the Stern-Volmer equation adopts more complicated forms. In our case the modified Stern-Volmer equation giving the best fitting function of the experimental data is in the form

$$\frac{I_0}{I} = \left[\sum_{i=1}^{n} \frac{f_{(i)}}{(1 + K_{SV(i)}[Q])}\right]^{-1}. \tag{4}$$

Equation (4) is an extension of the linear Stern-Volmer equation, where it is assumed that n fluorescent multiple species, independent and not interacting one another, are present in the sensing material.[46] In the equation (i) denotes a specific K_{SV} value per species, and $f_{(i)}$ is the fractional intensity of each emitting species, which is a function of concentration, quantum yield and emission spectrum of each individual PL species.

Rigorously speaking, this subject is usually referred to optical sensing by molecular fluorescence, where the concept of "emitter" is well defined and the interaction with a gas molecule results localized in the space. In our case the "emitter" is the quantum state (exciton state and/or electron defect states) and the interaction occurs at the solid surface, between the gas molecules and such states.[47] The experimental values of $\frac{I_0}{I}$ versus [NO_2] and the best fit curves (continuous lines) are reported in Fig. 5(b). In our fitting procedure the best fit is obtained in the case of $n = 2$. All the others fitting parameters are reported in Table II.

The results of the fitting procedure suggest that there are two different "emitters" in each band, and one of them is independent of gas concentration and consequently, the corresponding K_{SV} constant is zero. This means that this emitter species is unaffected by the gas molecules and thus unquenched. The K_{SV} constant of the gas-dependent emitter is almost the same in excitonic and defect emission bands, indicating that the involved process is similar in both bands. Furthermore it results that the unquenched PL fraction (contribution to the emission signal coming from the gas-independent emitter) is larger than the quenched one (contribution from the gas-dependent emitter), both in the excitonic (76% versus 24%) and in the defect emission band (91%

TABLE II. Fitting parameters values of the modified Stern-Volmer equation $\frac{I_0}{I} = \left[\sum_{i=1}^{n} \frac{f_{(i)}}{(1+K_{SV(i)}[Q])}\right]^{-1}$ where it is assumed that n fluorescent multiple species, independent and not interacting one another, are present in the sensing material. In the equation (i) denotes a specific K_{SV} value per species, and $f_{(i)}$ is the fractional intensity of each emitting species. The fitting parameters of equation $\frac{I_0}{\Delta I} = \frac{1}{R[Q]} = \frac{1}{f_a K_{SV}^q [Q]} + \frac{1}{f_a}$, where I_0^q and I_0^{un} are the PL intensities of the quenched and unquenched emitters, respectively, and f_a is the quenchable fraction of the initial PL signal, namely, $f_a = \frac{I_0^q}{I_0^q + I_0^{un}}$, are also shown for comparison on the right side.

Fitting parameters	f_1	$K_{SV(1)}$ ppm^{-1}	f_2	$K_{SV(2)}$ ppm^{-1}	f_a	K_{SV}^q
Excitonic band	0.24 ± 0.05	0.008 ± 0.004	0.76 ± 0.06	0	0.24 ± 0.02	0.008 ± 0.001
Defect band	0.09 ± 0.02	0.010 ± 0.007	0.91 ± 0.02	0	0.089 ± 0.008	0.010 ± 0.002

versus 9%), as we can see in Table II. Obviously, in the excitonic band the quenched PL fraction results more important than in the defect one (24% versus 9%). In particular, the ratio of quenched PL fraction of excitonic and defect band $\frac{f^1_{exc}}{f^1_{def}} = 2.7 \pm 1.0$ results, as expected, comparable to the ratio between the corresponding sensing responses $\frac{R_{exc}}{R_{def}} = 2.2 \pm 0.2$ (calculated as average value of $\frac{R_{exc}([Q])}{R_{def}([Q])}$ ratio, obtained in the investigated [Q] range).

The presence of an emitter that results independent of gas concentration can be justified by considering it as an emitter that is not accessible to the quencher species. From this point of view, this model allows us to distinguish between the accessible and the inaccessible fraction of the total PL emission. On the basis of the SEM cross sectional results, we deduce that the quenchable emitters correspond to the emitter states of the nanowires whereas the unquenchable states are the bulk states of the buffer layer, which can strongly contribute to PL emission but it is hardly accessible to the NO_2 gas molecules. The role of the sample morphology on the sensing response is frequently discussed in literature.[48,49] On this purpose, in particular, Valerini *et al.* has shown that film morphology in nanostructured ZnO films influences the NO_2 gas sensing responses, showing an improvement of the sensor response in nanostructures with high aspect ratio and large total surface exposed to gas adsorption.[29] This is the case of our samples, where the nanowires have a large surface to volume ratio and consequently, they can be the main structures involved in the quenching processes.

In this frame it deserves to point out that the PL signal I_0 before the gas interaction, can be written as $I_0 = I_0^q + I_0^{un}$, where I_0^q and I_0^{un} are the PL intensities of the quenched and unquenched emitters, respectively. As a consequence, the PL intensity I_{gas}, resulting from the quenching processes, by means of Eq. (3), is

$$I_{gas} = \frac{I_0^q}{1 + K_{SV}^q [Q]} + I_0^{un}, \tag{5}$$

where K_{SV}^q is the Stern-Volmer quenching constant of the accessible emitter.[46] Then it results $I_0 - I_{gas} = \Delta I = I_0^q \left(\frac{K_{SV}^q [Q]}{1 + K_{SV}^q [Q]} \right)$ that can be rewritten in a more usual way for sensors applications

$$\frac{I_0}{\Delta I} = \frac{1}{R[Q]} = \frac{1}{f_a K_{SV}^q [Q]} + \frac{1}{f_a}, \tag{6}$$

where f_a is the quenchable fraction of the initial PL signal, namely, $f_a = \frac{I_0^q}{I_0^q + I_0^{un}}$. The plots of $\frac{1}{R}$ versus $\frac{1}{[NO_2]}$ for the two emission bands and the best fit (continuous line) by using Eq. (6), are shown in Fig. 5(c), which evidences that the expected linear dependence is verified. The values of K_{SV}^q and f_a, resulting from the fitting procedure and reported in the last two columns of Table II, are similar to the previous ones, obtained by using the modified Stern-Volmer equation.

Furthermore we observe that, concerning the K_{SV} attribution, namely the assignment of the static or dynamic quencher behavior, a comparison between PL intensity and PL lifetime variations is required, but this is not the aim of this work. Nevertheless we report that recently it has been shown that PL quenching in SnO_2 nanobelts and nanowires, induced by NO_2 gas, does not modify the PL lifetime, suggesting the presence of static quenching where the NO_2 gas, acting as an electron trapper, influences the number of recombination events, but not their dynamics.[20,47] Time resolved PL measurements in presence of 30 ppm of NO_2 gas molecules have been performed also in ZnO nanowires. In particular, Baratto *et al.*[50] have shown that during the gas–solid interaction the defect emission band lifetime (in the case of 3.5 eV excitation, lower than the band edge energy) does not vary and a surface static quenching model has been proposed.

Finally, in order to verify the response reproducibility and to exploit the presence of saturation processes, the samples were exposed at the highest gas concentration (115 ppm) for three gas/recover cycles. The typical dynamic responses are reported in Fig. 6. Using the fitting procedure described for the data in Fig. 4, we observe that

a. The response (recovery) time and response R in the signal dynamics of both excitonic and defect band do not change in the different cycles and they are also the same of the previous measurements performed at 115 ppm.
b. The contribution of the slow process results reduced as the cycles number increases, from a largest contribution of about 3% in the case of response/recovery signal of exciton band, down to a 0.4% of response/recovery signal of defect band.
c. As the cycle number increases, the PL signal does not recover the baseline value, thus indicating that a partial irreversibility appears in the interaction processes.

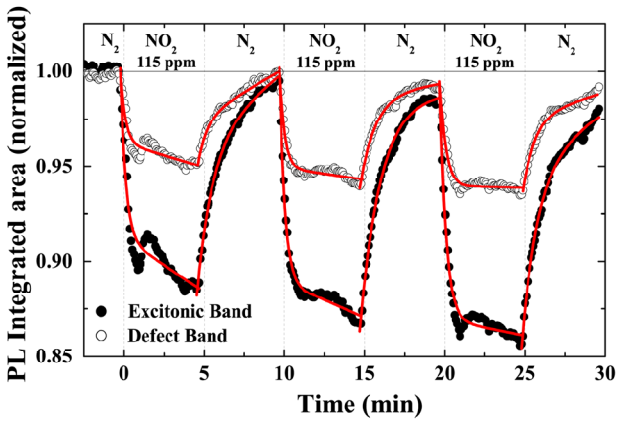

FIG. 6. Optical sensing measurements at 115 ppm NO_2 gas concentration (total flow of 50 ml/min) and at nitrogen recovery atmosphere, for excitonic (filled circle) and defect emission (empty circle) band of the sample. The best fits (continuous lines) obtained by the fitting function of each quenching/recovery cycle $I = A\exp\left[\frac{-(t-t_0)}{\tau}\right] + Bt + y_0$, where I stands for the integrated photoluminescence intensity, t represents the time, t_0 is the time corresponding to the edge of quenching/recovery cycle, τ is the time constant of the exponential process, y_0 is an offset fit parameter, are also shown.

In particular the difference observed between the baseline value I_{BV} and the recovered signal I_{rec} observed at the edge of the cycle, normalized to the baseline value $\left(\Delta I = \frac{I_{BV} - I_{rec}}{I_{BV}}\right)$, increases as the cycle number increases from 0.5% (0.1%) to 2% (1%) in exciton (defect) emission band cycles, and it results comparable in the two bands if normalized to the response value. This observation denotes that the irreversibility is comparable for the two bands and that it increases in the subsequent cycles. The irreversibility of the process can be simply associated to the interaction mechanism between gas molecules and sample surface and in particular, to the decrease of the number of suitable sites involved in the interaction process, due to an incomplete reversibility of the adsorption process.

Finally, concerning the response signal at high gas concentration, we observe that it presents an oscillation around the equilibrium value, more evident in the first cycle, related to the instability of the system. At this high gas concentration, in fact, the stabilization of adsorption and desorption processes of the gas molecules at the sample surface is expected to be complex and then the equilibrium can be reached slowly. This effect is more evident in excitonic band, which presents the larger response to the gas interaction.

IV. CONCLUSIONS

The optical sensing properties of ZnO thick nanostructured films, grown by VPD, toward NO_2 gas molecules have been investigated. The quenching/restoring of the PL signal in presence/absence of the analyte in excitonic and defect emission bands has been detected and analyzed. The sensing response is larger in the excitonic band than in the defect one and irreversibility ($\leq 2\%$) of the response appears only at the highest gas concentration (115 ppm) and only after more exposure cycles. We showed that the integrated PL signal decreases/increases mainly with an exponential behavior as a function of time, during the gas analyte/recovery atmosphere exposure, with a response/recovery time of few minutes, which results independent of gas molecules concentration and emission band. In addition, in the response/recovery signal a further decrease/increase, ascribed to a slow interaction processes and showing a linear trend, is also present but, due to its very low contribution (1-3%), can be neglected. The resulting calibration curve follows a sub-linear trend and a deeper analysis shows that the response signal results from the superimposition of quenched and unquenched emission, coming, respectively, from the nanowires and the "bulk" emission states of the samples. We demonstrate that the quenchable fraction of the PL signal follows the Stern-Volmer equation. The presence of an unquenchable signal, due to the high density of nanostructures, which does not allow the interaction between the gas molecules and the buffer layer, confirms the very important role of the sample morphological features in the sensing response.

ACKNOWLEDGMENTS

The authors would like to thank Mrs. C. Martucci for the preparation of the sample and Mr. F. Casino and Mr. G. Montagna for technical assistance and realization of the experimental set-up for optical measurement in controlled atmosphere.

[1]S.H. Park, S. H. Kim, and S.W. Han, Nanotechnology **18**, 055608 (2007).
[2]J. Bao, M. A. Zimmler, F. Capasso, X. Wang, and Z. F. Ren, Nano Letters **6**, 1719 (2007).
[3]D. Yu, Y. Chen, B. Li, X. Chen, M. Zhang, F. Zaho, and S. Ren, Appl. Phys. Lett. **91**, 091116 (2007).
[4]L. J. Bie, X. Yan, J. Yin, Y. Duan, and Z. Yuanet, Sens. Actuators B **126**, 604 (2007).
[5]E. Comini, G. Faglia, M. Ferroni, and G. Sberveglieri, Appl. Phys. A **88**, 45 (2007).
[6]C. C. Li, Z. F. Du, L. M. Li, H. C. Yu, Q. Wan, and T. H. Wanget, Appl. Phys. Lett. **91**, 32101 (2007).
[7]A. Wei, X. W. Sun, and J. X. Wang, Appl. Phys. Lett. **89**, 123902 (2006).
[8]S. C. Minne, S. R. Manalis, and C. F. Quate, Appl. Phys. Lett. **67**, 3918 (1995).
[9]M. H. Huang, S. Mao, H. Feick, H. Yan, Y. Wu, H. Kind, E. Weber, R. Russo, and P. Yang, Science **292**, 1897 (2001).
[10]D. J. Gargas, M. E. Toimil-Molares, and P. Yang, J. Am. Chem. Soc. **131**, 2125 (2009).
[11]Y. Gu, I. L. Kuskovsky, M. Yin, S. O'Brien, and G. F. Neumark, Appl. Phys. Lett. **85**, 3833 (2004).
[12]D. Haranath, S. Sahai, A. G. Joshi, B. K. Gupta, and V. Shanker, Nanotechnology **20**, 425701 (2009).
[13]A. G. Joshi, S. Sahai, N. Gandhi, Y. G. R. Krishna, and D. Haranath, Appl. Phys. Lett. **96**, 123102 (2010).
[14]X. L. Cheng, H. Zhao, L. H. Huo, S. Gao, and J. G. Zhao, Sens. Actuators B **102**, 248(2004).
[15]P. D. Batista and M. Mulato, Appl. Phys. Lett. **87**, 143508 (2005).
[16]C. S. Rout, S. H. Krishna, S. R. C. Vivekchand, A. Govindaraj, and C. N. R. Rao, Chem. Phys. Lett. **418**, 586 (2006).
[17]H. Lim, D. Y. Lee, and Y. J. Oh, Sens. Actuators A **125**, 405 (2006).
[18]H. Xu, X. Liu, D. Cui, M. Li, and M. Jiang, Sens. Actuators B **114**, 301 (2006).
[19]G. Sberveglieri, C. Baratto, E. Comini, G. Faglia, M. Ferroni, A. Ponzoni, and A. Vomiero, Sens. Actuators B **121**, 208 (2007).
[20]A. Bismuto, S. Lettieri, P. Maddalena, C Baratto, E Comini, G Faglia, G Sberveglieri, and L. Zanotti, J. Opt. A: Pure Appl. Opt. **8**, S585 (2006).
[21]C. de Julián Fernández, M. G. Manera, G. Pellegrini, M. Bersani, G. Mattei, R. Rella, L. Vasanelli, and P. Mazzoldi, Sens. Actuators B **130**, 531 (2008).
[22]T. Mazingue, L. Escoubas, L. Spalluto, F. Flory, G. Socol, C. Ristoscu, E. Axente, S. Grigorescu, I. N. Mihailescu, and N. A. Vainos, J. Appl. Phys. **98**, 74312 (2005).
[23]A. O. Dikovska, P. A. Atanasov, A. T. Andreev, B. S. Zafirova, E. I. Karakoleva, and T. R. Stoyanchov, Appl. Surf. Sci. **254**, 1087 (2007).
[24]W. An, X. Wu, and X. C. Zeng, J. Phys. Chem. C **112**, 5747 (2008).
[25]J. D. Prades, A. Cirera, and J. R. Morante, Sens. Actuators B **142**, 179 (2009).
[26]A. Tsukazaki, A. Ohtomo, M. Kawasaki, T. Makino, C. H. Chia, Y. Segawa, and H. Koinuma, Appl. Phys. Lett. **84**, 3858 (2004).
[27]C. H. Wu and H. Niki, Environ. Sci. Technol. **9**, 46 (1975).
[28]M. Wojciechowska and S. Lomnicki, Clean Prod. Processes **1**, 237 (1999).
[29]D. Valerini, A. Cretì, A. P. Caricato, M. Lomascolo, R. Rella, and M. Martino, Sens. Actuators B **145**, 167 (2010).
[30]A. Taurino, M. Catalano, A. Cretì, M. Lomascolo, C. Martucci, and F. Quaranta, Mater. Sci. Eng. B **172**, 225 (2010).
[31]D. C. Reynolds, D. C. Look, B. Jogai, C. W. Litton, G. Cantwell, and W. C. Harsch, Phys. Rev. B **60**, 2340 (1999).
[32]J. F. Muth, R. M. Kolbas, A. K. Sharma, S. Oktyabrsky, and J. Narayan, J. Appl. Phys. **85**, 7884 (1999).
[33]J. A. Sans, A. Segura, M. Mollar, and B. Mari, Thin Solid Film **453–454**, 251 (2004).
[34]W. I. Park, Y. H. Jun, S. W. Jung, and G.-C. Yi, Appl. Phys. Lett. **82**, 964 (2003).
[35]Q. X. Zhao, M. Willander, R. E. Morjan, Q-H. Hu, and E. E. B. Campbell, Appl. Phys. Lett. **83**, 165 (2003).

[36]B. P. Zhang, N. T. Binh, Y. Segawa, Y. Kashiwaba, and K. Haga, Appl. Phys. Lett. **84**, 586 (2004).
[37]Z. W. Liu, C. K. Ong, T. Yu, and Z. X. Shen, Appl. Phys. Lett. **88**, 053110 (2006), and references therein.
[38]W. S. Shi, B. Cheng, L. Zhang, and E. T. Samulski, J. Appl. Phys. **98**, 083502 (2005).
[39]B. P. Zhang, N. T. Binh, Y. Segawa, K. Wakatsuki, and N. Usami, Appl. Phys. Lett. **83**, 1635 (2003).
[40]Y. P. Varshni, "Temperature dependence of the energy gap in semiconductors," Physica **34**, 149 (1967).
[41]T. Andelman, Y. Gong, M. Polking, M. Yin, I. Kuskovsky, G. Neumark, and S. O'Brien, J. Phys. Chem. B **109**, 14314 (2005).
[42]Z. W. Liu, C. K. Ong, T. Yu, and Z. X. Shen, Appl. Phys. Lett. **88**, 053110 (2006), and references therein.
[43]M. K. Lee and H. F. Tu, J. Appl. Phys. **101** 126103 (2007).
[44]N. Han, P. Hu, A. Zuo, D. Zhang, Y. Tian, and Y. Chen, Sens. Actuators B **145**, 114 (2010).
[45]G. Orellana, in Optical Chemical Sensors, NATO Science Series - II. Mathematics, Physics and Chemistry – Vol. 224, edited by F. Baldini, A. N. Chester, J. Homola, and S. Martellucci (Springer, 2006), pp. 99–116.
[46]C. D. Geddes, Review Article – Meas. Sci. Technol. **12**, R53 (2001).
[47]S. Lettieri, A. Setaro, C. Baratto, E. Comini, G. Faglia, G. Sberveglieri, and P. Maddalena, New J. Phys. **10**, 043013 (2008).
[48]B. Shouli, C. Liangyuan, L. Dianqing, Y. Wensheng, Y. Pengcheng, L. Zhiyong, C. Aifan, and C. C. Sens, Actuators B **146**, 129 (2010).
[49]Y. Lingmin, F. Xinhui, Q. Lijun, M. Lihe, and Y. Wen, Appl. Surf. Sci. **257**, 3140 (2011).
[50]C. Baratto, S. Todros, G. Faglia, E. Comini, G. Sberveglieri, S. Lettieri, L. Santamaria, and P. Maddalena, Sens. Actuators B **140**, 461 (2009).